Microscopic coloured quark-dynamics in the soft non-perturbative regime – Description of hadron formation in relativistic S+Au collisions at CERN

S. Scherer†,* M. Hofmann, M. Bleicher, L. Neise, H. Stöcker†, W. Greiner†

4. June 2001

† Institut für Theoretische Physik, J.W.Goethe-Universität, Robert-Mayer-Str. 8-10, D-60054 Frankfurt am Main, Germany

Abstract

The quark-molecular-dynamics model is used to study microscopically the dynamics of the coloured quark phase and the subsequent hadron formation in relativistic S+Au collisions at the CERN-SPS. Particle spectra and hadron ratios are compared to both data and the results of hadronic transport calculations. The non-equilibrium dynamics of hadronization and the loss of correlation among quarks are studied.

1 Introduction

The relativistic heavy ion collider (RHIC) at Brookhaven National Laboratory and the running Pb+Pb program at the CERN-SPS aim to explore the phase diagram of hot and dense matter near the quark gluon plasma (QGP) phase transition [1]. The QGP is a hypothetical state in which the individual hadrons dissolve into a gas of free (or almost free) quarks and gluons in strongly compressed and heated matter. The energy- and baryon densities

*To whom correspondence should be addressed (scherer@th.physik.uni-frankfurt.de)

achievable in heavy ion collisions sensitively depend on the extend to which the nuclei are stopped during penetration; they also depend on mass number and bombarding energy.

However, a detailed understanding of the quark dynamics and the subsequent parton-hadron phase transition is still missing. First exploratory attempts have been made using hydrodynamical simulations, like one-fluid hydro [2] and three-fluid hydrodynamics [3, 4]. It has been found that the results of these investigations are strongly influenced by the freeze-out definition and the non-equilibrium features encountered in heavy ion reactions [3].

Very recently it has been tried to circumvent the freeze-out problem by coupling the hydrodynamical simulation to the semi-hadronic transport model UrQMD [5]. A detailed microscopic simulation of the quark phase and of the hadronization, however, is still missing.

Attempts to simulate the dynamics of the hot and dense region within the VNI model [6] suffer from the non-perturbative origin of the quark-quark interaction at SPS and RHIC energies – this has already been pointed out by Müller and Harris, who stressed that it is important to realize that the QGP is a strongly interacting gas of quarks and gluons at low momentum transfer $q^2 < q^2_{\rm CSB}$ (CSB = Chiral symmetry breaking) [7]. Even at RHIC energies leading order (and next-to leading order) perturbative QCD (pQCD) seems to be inapplicable to understand the heated and compressed system encountered as shown in [8, 9].

In this paper we present the first microscopic model calculation of the quark dynamics in the non-perturbative regime dubbed the Quark Molecular Dynamics Model (qMD) [10, 11]. The model is applied to the dynamics of the expanding fireball in relativistic S+Au collisions at CERN.

2 Discussion of the model

The qMD model [10, 11] is a semi-classical model which mimics the properties of non-Abelian QCD by the means of a two-body colour potential between quarks and antiquarks. In addition, a dynamical hadronization criterion is defined which allows for the consecutive migration from quark to hadronic degrees of freedom. A very similar model has been used before to study the spontaneous generation of density perturbations in the early universe triggered by the hadronization of the primordial quark–gluon plasma [12].

The coloured and flavoured quarks (and antiquarks) are treated as classical particles interacting via a Cornell potential with colour matrices [13]. This interaction provides an effective description of the non-perturbative, soft gluonic part of QCD.

The model does not treat the explicit dynamics and fragmentation of hard gluons. In any application of the model the validity of this approximation has to be checked.

Using these assumptions, the model Hamiltonian reads

$$\mathcal{H} = \sum_{i=1}^{N} \sqrt{p_i^2 + m_i^2} + \frac{1}{2} \sum_{i,j} C_{ij} V(|\mathbf{r}_i - \mathbf{r}_j|)$$

where N counts the number of particles in the system. The particles are quarks or antiquarks carrying a fixed colour charge – red, green, blue for quarks, anti-red- anti-green and anti-blue for antiquarks. Four quark flavours (u, d, s, c) with current masses $m_u = m_d = 10$ MeV, $m_s = 150$ MeV and $m_c = 1.5$ MeV are considered. In order to allow for a later mapping of quark clusters to hadronic states, the particles carry spin and isospin quantum numbers. The confining properties of the potential $V(r)$ are ensured by a linear increase at large distances r. At short distances, the strong coupling constant α_s becomes small, yielding a Coulomb-type behaviour as in QED. For this colour Coulomb potential plus the confining part we use the well known Cornell-potential [14]

$$V(r) = -\frac{3}{4} \frac{\alpha_s}{r} + \kappa\, r \ ,$$

which has successfully been applied to meson spectroscopy. For infinite quark masses this inter-quark potential has also been found in lattice calculations over a wide range of quark distances [15]. For small quark masses, retardation and chromomagnetic effects should be included. This is neglected in the present work. However, the linear behaviour at large distances seems to be supported by the success of the string model even for zero quark masses [16].

By fixing the colour of each quark or antiquark, we restrict ourselves to the approximation that there are no interactions changing the colour of quarks. The use of this approximation – which breaks, of course, the full colour gauge symmetry – is motivated by the physical picture behind the maximal Abelian gauge of QCD [17] which gives, at the same time, a justification for the use of the linearly increasing potential. In this gauge, there remains a residual gauge

Table 1: Colour matrix elements of the 36 different elementary colour combinations of the quarks. The matrix elements can be obtained from the scalar products of the corresponding weight vectors

$C_c^{\alpha\beta}$	R	G	B	$\overline{B}$	$\overline{G}$	$\overline{R}$
R	-1	$+\frac{1}{2}$	$+\frac{1}{2}$	$-\frac{1}{2}$	$-\frac{1}{2}$	$+1$
G	$+\frac{1}{2}$	-1	$+\frac{1}{2}$	$-\frac{1}{2}$	$+1$	$-\frac{1}{2}$
B	$+\frac{1}{2}$	$+\frac{1}{2}$	-1	$+1$	$-\frac{1}{2}$	$-\frac{1}{2}$
$\overline{B}$	$-\frac{1}{2}$	$-\frac{1}{2}$	$+1$	-1	$+\frac{1}{2}$	$+\frac{1}{2}$
$\overline{G}$	$-\frac{1}{2}$	$+1$	$-\frac{1}{2}$	$+\frac{1}{2}$	-1	$+\frac{1}{2}$
$\overline{R}$	$+1$	$-\frac{1}{2}$	$-\frac{1}{2}$	$+\frac{1}{2}$	$+\frac{1}{2}$	-1

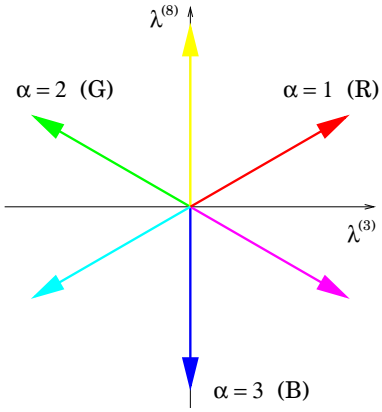

freedom corresponding to the two diagonal gluons. The non diagonal gluons become massive [18], contributing only over very short ranges in the order 0.2 – 0.3 fm [19, 20]. Simultaneously, the colour fields of the diagonal gluons are quenched to flux tubes via the dual Meissner effect [21]. This mechanism then yields the linear increase of the colour potential with distance. The remaining colour interaction contains the diagonal gluons which carry no colour and therefore do not change colour.

The colour matrix elements C_{ij} regulate the sign and relative strength of the interaction between two quarks/antiquarks, respectively, depending on the colour combination of the pair. The matrix C_{ij} in the short range colour interaction potential between quarks, $V_{\rm colour} = -C_{ij}\frac{3}{4}\frac{\alpha}{r}$, can be calculated from one-gluon exchange of the quark-gluon interaction of the QCD Lagrangian,

$$\mathcal{L}_{\rm int} = \frac{g}{2}\,\bar{\Psi}\lambda_a\gamma_\mu\Psi G_a^\mu\ .$$

Using the standard fundamental representation of $SU(3)_{\rm colour}$ for the quarks and the adjoint representation for the gluons,

$$\vec{q}_R = \begin{pmatrix}1\\0\\0\end{pmatrix},\quad \vec{q}_G = \begin{pmatrix}0\\1\\0\end{pmatrix},\quad \vec{q}_B = \begin{pmatrix}0\\0\\1\end{pmatrix},$$

$$T^a = \frac{1}{2}\lambda^a, \quad a = 1, \ldots, 8$$

where λ_a are the Gell-Mann matrices, and separating the quark wave function in the colour and Dirac parts, the interaction amplitude also splits in colour and Dirac parts:

$$\mathcal{M}_{\alpha\alpha'\beta\beta'} \sim \bar{\psi}_1\gamma_\mu\psi_1 D^{\mu\nu}(q)\psi_2\gamma_\nu\psi_2\, \vec{q}^{\,\dagger}_{\alpha'}\lambda^a\vec{q}_\alpha\delta_{ab}\vec{q}^{\,\dagger}_{\beta'}\lambda^b\vec{q}_\beta \ .$$

Here, $\mathcal{D}^{\mu\nu}_{ab}(q) = D^{\mu\nu}(q)\delta_{ab}$ is the gluon propagator, and α and β represent the colour charges of the incoming quarks, α' and β' of the outgoing quarks in the one-gluon exchange diagram. Collecting the colour parts in a colour factor

$$C^{\rm c}_{\alpha\alpha'\beta\beta'} = \frac{3}{4}\sum_{a=1}^{8} \vec{q}^{\,\dagger}_{\alpha'}\lambda^a\vec{q}_\alpha\, \vec{q}^{\,\dagger}_{\beta'}\lambda^a\vec{q}_\beta = \frac{3}{4}\sum_{a=1}^{8}(\lambda^a)_{\alpha\alpha'}\,(\lambda^a)_{\beta\beta'} \ ,$$

one can calculate the net amplitude by summing over all possible combinations of in- and outgoing colours. In the maximally Abelian gauge, only the the diagonal gluons, described by the commutating Gell-Mann matrices λ_3 and λ_8 from the Cartan subalgebra of $SU(3)_{\rm colour}$, contribute over larger distances. In this approximation the total colour matrix for quark-quark interactions then is given by

$$C^{\rm c}_{\alpha\beta} = \frac{3}{4}\sum_{a=3,8}(\lambda^a)_{\alpha\alpha}(\lambda^a)_{\beta\beta} = \vec{w}^{\,\mathsf{T}}_\alpha\vec{w}_\beta \ ,$$

where

$$\vec{w}_\alpha = \frac{\sqrt{3}}{2}\begin{pmatrix} (\lambda^3)_{\alpha\alpha} \\ (\lambda^8)_{\alpha\alpha} \end{pmatrix}, \quad \alpha = 1,2,3\ (R,G,B)$$

are the normalised weight vectors corresponding to the three quark colours in (λ^3, λ^8) space. Imposing a factor -1 at each antiquark vertex in colour space yields the colour matrix elements for the different colour combinations as collected in table 1. They can easily be read off as the scalar products of the weight vectors corresponding to the three colours or anticolours, respectively. Positive values indicate attractive, negative repulsive interactions.

The classical time evolution of the (anti)quark system as given by the Hamiltonian yields colourless clusters of (a) three quarks with different colours or (b) a quark and an antiquark with opposite colours. This is a consequence of the interplay between the attractive and repulsive interactions in the system which trigger this segregation. These quark clusters are mapped on

hadronic resonance states according to energy-momentum conservation and the known spin and isospin quantum numbers of the quarks in the cluster. In our model, the resonance states do not interact any more with the system (there is no hadronic rescattering) - they just decay into stable hadrons.

It should be noted that the qMD model includes the possible creation of quark-antiquark pairs out of the vacuum. However, this is a process which is rare in systems with no large fluctuations in colour charge. We will come back on this point in our application of the model to heavy ion collisions.

A detailed discussion of the model, including the clustering and hadronization procedure, resulting thermal properties and the Equation of State, and analytic test cases are found in [10, 11].

There are, of course, several other approaches to the dynamical description of the quark degrees of freedom in a hot and dense quark system. In [22, 23], a simulation based on the Nambu-Jona-Lasinio model has been presented, where quarks are propagated on classical trajectories while their effective masses are calculated self-consistently according to the NJL equations of motion. Hadron production is driven by qq and qh collisions. Unfortunately, this approach does not provide confinement and therefore is less suited for the investigation of heavy-ion collisions. A fully gauge symmetric treatment of the colour degrees of freedom of the quarks including colour rotations has been presented in [24]. However, in this approach it is difficult to regain colourless hadrons out of the quark system. It is also possible to treat the colour field as a dynamical background field whose source are the quarks [25]. This approach (while also fixing the quark colour) is less idealised than the one presented in this paper, but the numerics is still too time consuming to treat systems of the size of fireballs from heavy ion collisions.

3 Application to heavy ion collisions at the SPS

We now apply the qMD model to study the expansion and hadronization of the fireball created in heavy ion collisions between S and Au nuclei at the SPS.

The initial state of the quark dynamics is generated by a transport simulation with hadronic and string degrees of freedom (in this paper the UrQMD model [26] is used—other models can also be applied). The initial nuclei are

propagated within the transport simulation until a critical energy density is reached. In the investigated collisions, we assume the dissolution of the hadronic degrees of freedom at an energy density of 1 GeV/fm^{-3} in line with recent lattice calculations [27]. This energy density is reached at full overlap, i. e. 1.5 fm/c after the begin of the interaction. At this time all hadrons (mesons and baryons) are dissolved and all newly produced $q\bar{q}$ pairs from the decaying colour fields are used as input of the quark Molecular Dynamics model.

In the study presented here, it is justified to omit the explicit dynamics and fragmentation of thermal gluons due to their small number. The number N of gluons in the interaction region of volume V and temperature T can be estimated by:

$$N = Vg \int \frac{\mathrm{d}^3 p}{(2\pi)^3} \frac{1}{\exp(|p|/T) - 1} = V \frac{g}{\pi^2} \zeta(3) T^3 \quad ,$$

with the degeneracy $g = 16$. Assuming Bjorken-like initial expansion and a temperature of $T = 200$ MeV we expect 88 thermal gluons in our simulation at the moment of full overlap, carrying approximately 10% of the entropy of the system. Due to the cooling of the system at expansion, this provides an estimate for an upper bound on the number of thermal gluons. Thus, the additional fragmentation of these gluons is not expected to change the calculated yields and ratios significantly and has been left out in the present calculations. The contribution of hard gluons is negligible at SPS energies.

The results of the qMD simulation of a S+Au collision are visualised in two MPEG movies. The first movie depicts the time evolution of a collision in the plane of the beam axis (horizontal axis, z) and the impact parameter axis (vertical axis, x). The second movie shows the same event, but this time as seen by an observer on the beam axis (the horizontal axis in this movie is the impact parameter axis, x). The second movie shows nicely the wobbling motion of the quarks and antiquarks (coloured spheres) forming clusters of two or three (carrying colour and anti-colour or three different colours, respectively) which are then considered as hadrons (grey spheres).

Figure 1 also shows the space-time evolution of the quarks and antiquarks (thick, coloured dots) and hadrons (small white dots): The central zone of the collision is filled up with (anti)quarks that re-arrange themselves to colour neutral clusters. These clusters are then decaying into physical hadron states.

Figure 2 depicts the evolution of the rapidity densities of baryons (dotted lines), mesons (dashed lines) and (anti)quarks (full lines). The remnants of

the gold nucleus re-hadronize immediately. The quarks at central rapidities start to form mesons. After 20 fm/c the quarks have re-combined to hadrons and the collision ceases.

The time evolution of the particle multiplicities (Figure 3) shows that the production of hadronic clusters starts immediately after the beginning of the collision. The hadron multiplicity rises steeply at $t = 1.5$ fm/c, while the quark multiplicity goes down. The steep rise in the hadron abundance is due to the rapid expansion of the initial hot and dense system. At later times, the multiplicity curves saturate. There could be two reasons for this flattening: either the back reaction $hh \rightarrow q\bar{q}$ becomes important due to the large abundance of pions, or the particle density becomes to low to cause further collision-induced changes of the multiplicities. Since the remaining number of unbound quarks vanishes with the saturation of the hadron multiplicity, we conclude in line with the findings in [22] that the hadron numbers saturate due to the breakup of the fireball rather than the approach to chemical equilibrium in the $hh \leftrightarrow q\bar{q}$ channel.

Note that the number of final hadrons is larger then the number of 2- and 3-clusters which can be formed out of the quarks and antiquarks in the initial state. This is caused by the decays of the hadronic clusters. As mentioned before, qMD includes the possible dynamical production of $q\bar{q}$ pairs in overcritical colour fields. However, in the present model, hadronization at SPS is basically driven by quark rearrangement: On average, only 0.1 quark-antiquark pairs per event are produced by string breakup in a S+Au collision. The reason is that by dissolving the hadronic content of UrQMD one start with a configuration which is colour neutral on longer scales. Thus, colour fluctuations large enough to yield strong colour fields which will then drag quark-antiquark pairs out of the vacuum are never reached. Moreover, strong fields are dynamically screened by the moving quarks.

Let us now confront the qMD results to experimental data. Figure 4 compares the calculated proton (full line), lambda (dotted line) and h^- rapidity densities to NA35 data (see [28] and references therein). A surprisingly good description of the measured data (symbols) over all rapidities by the non-equilibrium quark dynamics is found.

Figure 5 explores the the transverse expansion of the hadronizing quark system. The transverse momentum spectrum of negatively charged particles is compared to NA35 data. Overall good agreement is found.

Finally we want to investigate the hadro-chemical evolution and the behaviour of hadron ratios in the qMD model. Figure 6 displays the time de-

velopment of several hadron ratios in the course of the hadronization (shaded areas denote the measured ratios). The particle ratios stay nearly constant during the parton-hadron conversion. This may explain the success of statistical model analysis [29]. However, baryons seem to be produced in the later stage of the hadronization. The discrepancies between the ratios of p/π^+ and $(\Lambda_0 + \Sigma_0)/p$ obtained from our approach and the measured data can be understood from the missing hadronic rescattering in our approach. This can be seen by comparing the measured hadron ratios in figure 7 not only with the qMD calculation (diamonds) but also to ratios obtained with full UrQMD simulations (open circles).

While the proton to antiproton ratio remains unaltered as compared to the UrQMD calculation alone (and nearly one order of magnitude lower than the experimental value), ratios involving protons or antiprotons alone or the net proton number are by factors 2–5 higher in qMD than UrQMD, yielding a better fit to data for the $\bar{p}/\pi^-$ ratio, but an increasing overestimation for the p/π^+ and the $(p - \bar{p})/h^-$ ratio. Simultaneously, the ratio of $\Lambda/(p - \bar{p})$ drops against the value from UrQMD. Both trends can be understood as consequences of hadronic rescattering in the UrQMD model. Hadronic rescattering lowers the number of antiprotons in the final state, and, by inelastic baryon-baryon and antikaon-baryon collisions, yields a systematic population of hyperons at the expense of protons. These channels are not implemented in the present version of our qMD model. In qMD, delta resonances for example (which are abundant around the first 10 fm/c of the collision) cannot create hyperons and kaons by inelastic collisions, but eventually yield always nucleons and pions. As this simplification of the combined UrQMD+qMD approach with respect to a full UrQMD treatment shifts the calculated ratios away from the known experimental values, this can be seen as a clear sign for the importance of hadronic rescattering.

As the hadron ratios in the combined approach show differences due to missing rescattering and the transverse mass spectra and rapidity distribution of figures 5 and 4 can also be reproduced by the UrQMD model [26, 30], one may ask to which extent this combination of models may be useful or necessary.

The qMD approach can provide us with detailed information about the dynamics of the quark system and the parton-hadron conversion. Whenever a new hadron is formed, the correlation between the quarks clustering to build this hadron can be studied. The mean value of the path length these quarks have travelled within the quark phase from their points of origin until

the clustering point and the distance in space between the origins of the involved quarks can be studied.

Figure 8 shows the combined distribution of the mean path length travelled by the quarks and the original distance between the quarks forming a new hadron in S+Au collisions at SPS energies of 200 GeV/N. Quarks stemming from the same initial hadron correlation, propagating coherently and reclustering again to form the same hadron build up a large background at zero initial distance. The essence of this distribution is contained in figure 9 which shows the number distribution for the mean path travelled by quarks forming a hadron (a) from the same initial hadron (solid line) and (b) from different initial hadrons (dotted line).

One sees that the reclustering in (a) is quite quick: in this case a hadron is decomposed into two or three quarks, these quarks propagate a short distance of about 2.2 fm ("diffusion length" – marked by the grey box) and rehadronize again. The hadron formation follows an exponential decay of the quark cluster to hadrons with a decay length equal to the diffusion length of 2.2 fm.

On the other hand, the rearrangement of quarks to form new, different hadrons happens on a length scale of about 3 fm. Following this rearrangement, the clusters decay exponentially with a decay length of 4.8 fm.

A measure of the relative mixing within the quark system – and also for thermalization which means homogenisation of the population of phase space and complete loss of correlations – are the relative number of hadrons formed by quarks stemming from the same hadron correlation (rehadronization – these hadrons are dubbed "direct hadrons") versus hadrons formed by quarks stemming from different hadrons ("mixed hadrons"). The ratio r of mixed hadrons to the total number of hadrons formed from the quark system is $r = 0.574 \pm 0.008$ for the S+Au collision at 200 GeV/N. The Error is from statistics. A value of $r = 1$ would indicate complete rearrangement of quarks and thus complete loss of correlations in the quark system. Considering the presumed transition to the quark-gluon plasma in Pb+Pb collisions at 160 GeV/N, one would expect a much larger value of r.

We see that while global observables do not show large differences between hadronic calculations from UrQMD alone and our combined description using quark molecular dynamics, the easy rearrangement of quarks does indeed play a role and may hint to state of deconfined matter at the CERN SPS. Note that this rearrangement may be observed with the help of balance functions [31]. Such an analysis would, however, require better statistics.

4 Conclusion

In conclusion, we have used the Quark Molecular Dynamics Model (qMD) and investigated the non-equilibrium quark dynamics at SPS energies. The qMD has been coupled to the UrQMD model to generate the initial quark distributions. Good agreement with S+Au data at 200 GeV/N is found. This includes rapidity spectra, transverse momentum spectra and hadron ratios of mesons. While the missing rescattering in the qMD distorts the relative numbers of protons and hyperons, the coupled approach allows a detailed look at the dynamics of the quark system and the parton-hadron conversion. Our investigation shows that the parton-hadron phase transition in this model is mainly driven by quark re-arrangement. Quark-antiquark pair production is a rare process which needs strong colour fields which are, however, dynamically screened by the moving quarks.

Acknowledgements

This work is in part supported by the BMBF, GSI, DFG and Graduiertenkolleg "Theoretische und experimentelle Schwerionenphysik".

References

References

[1] Bass S A, Gyulassy M, Stöcker H, and Greiner W 1999 *J. Phys. G* **25** R1

[2] Rischke D H 1996 *Nucl. Phys.* **A610** 88c

[3] Brachmann J, Dumitru A, Maruhn J A, Stöcker H, Greiner W, and Rischke D H 1997 *Nucl. Phys.* **A619** 391

[4] Brachmann J, Soff S, Dumitru A, Stöcker H, Maruhn J A, Greiner W, and Rischke D H 2000 *Phys. Rev.* **C61** 024909

[5] Bass S A, Dumitru A, Bleicher M, Bravina L, Zabrodin E, Stöcker H, and Greiner W 1999 *Phys. Rev.* **C60** 021902

[6] Bass S A, Hofmann M, Bleicher M, Bravina L, Zabrodin E, Stöcker H, and Greiner W 1999 *Phys. Rev.* **C60** 021901

[7] Harris J W and Müller B 1996 *Ann. Rev. Nucl. Part. Sci.* **46** 71

[8] Bass S A and Müller B 1999 *Phys. Lett.* **B471** 108

[9] Fries R J, Müller B, Schäfer A, and Stein E 1999 *Phys. Rev. Lett.* **83** 4261

[10] Hofmann M, Scherer S, Bleicher M, Neise L, Stöcker H, and Greiner W 2000 *Phys. Lett.* **B478** 161

[11] Hofmann M, Scherer S, Bleicher M, Neise L, Stöcker H, and Greiner W *Preprint* nucl-th/9908031

[12] Crawford M and Schramm D N 1982 *Nature* **298** 538

[13] Isgur N and Paton J 1985 *Phys. Rev.* **D31** 2910

[14] Eichten E, Gottfried K, Kinoshita T, Kogut J, Lane K D, and Yan T M 1975 *Phys. Rev. Lett.* **34** 369

[15] Born K D, Laermann E, Sommer R, Zerwas P M, and Walsh T F 1994 *Phys. Lett.* **B329** 325

[16] Andersson B, Gustafson G, Ingelman G, and Sjostrand T 1983 *Phys. Rept.* **97** 31

[17] Ezawa Z F, Iwazaki I 1982 *Phys. Rev.* **D25** 2681

[18] Polikarpov M I 1997 *Nucl. Phys. Proc. Suppl.* **53** 134

[19] Amemiya K, Suganuma H 1999 *Nucl. Phys. Proc. Suppl* **83** 419

[20] Amemiya K, Suganuma H 1999 *Phys. Rev.* **D60** 114509

[21] 't Hooft G 1981 *Nucl. Phys.* **B190** 455

[22] Rehberg P, Bot L, and Aichelin J 1999 *Nucl. Phys.* **A653** 415

[23] Rehberg P, Bot L, and Aichelin J 1999 *Prog. Part. Nucl. Phys.* **42** 323

[24] Maruyama T and Hatsuda T 2000 *Phys. Rev.* **C61** 062201

[25] Traxler C T, Mosel U, and Biro T S 1999 *Phys. Rev.* **C59** 1620

[26] Bass S A, Belkacem M, Bleicher M, Brandstetter M, Bravina L, Ernst C, Gerland L, Hofmann M, Hofmann S, Konopka J, Mao G, Neise L, Soff S, Spieles C, Weber H, Winckelmann L A, Stöcker H, Greiner W, Hartnack C, Aichelin J, and Amelin N 1998 *Prog. Part. Nucl. Phys.* **41** 225

[27] Okamoto M (for the CP-PACS Collaboration) 1999 *Phys. Rev.* **D60** 094510

[28] Braun-Munzinger P, Stachel J, Wessels J P, and Xu N 1996 *Phys. Lett.* **B365** 1

[29] Rafelski J and Letessier J 1999 Proceedigns of the 15th Winter Workshop on Nuclear Dynamics, Park City, January 1999, W Bauer and G Westfall, Eds. *Preprint* hep-ph/9902365

[30] Bleicher M, Spieles C, Ernst C, Gerland L, Soff S, Stöcker H, Greiner W, and S.A. Bass 1999 *Phys. Lett.* **B447** 227

[31] Bass S A, Danielewicz P, and Pratt S 2000 *Phys. Rev. Lett.* **85** 2689

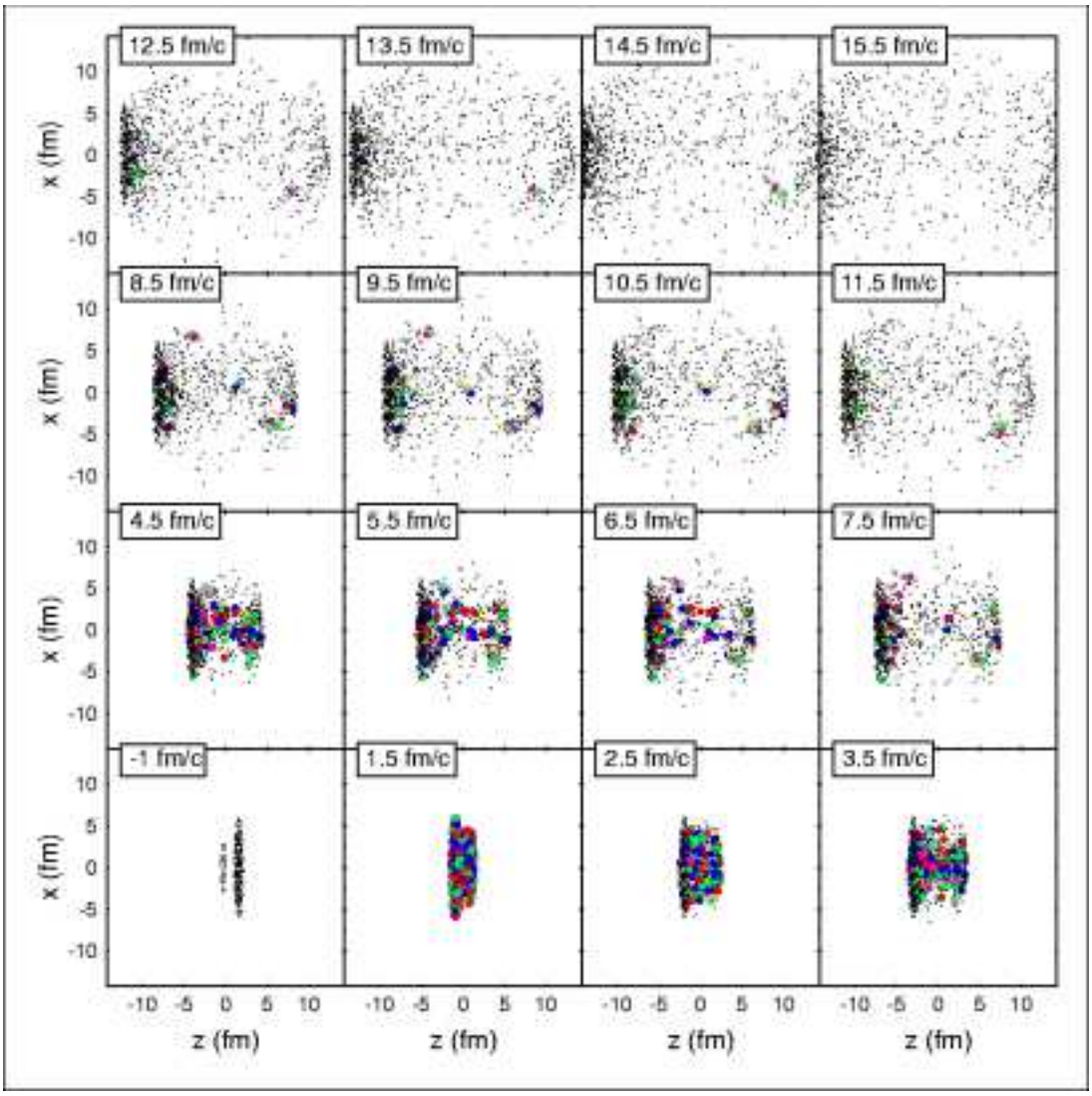

Figure 1: Time evolution of quarks, antiquarks and hadrons in a central S+Au at SPS (200 GeV/N). (z) is the beam axis and (x) the impact parameter direction.

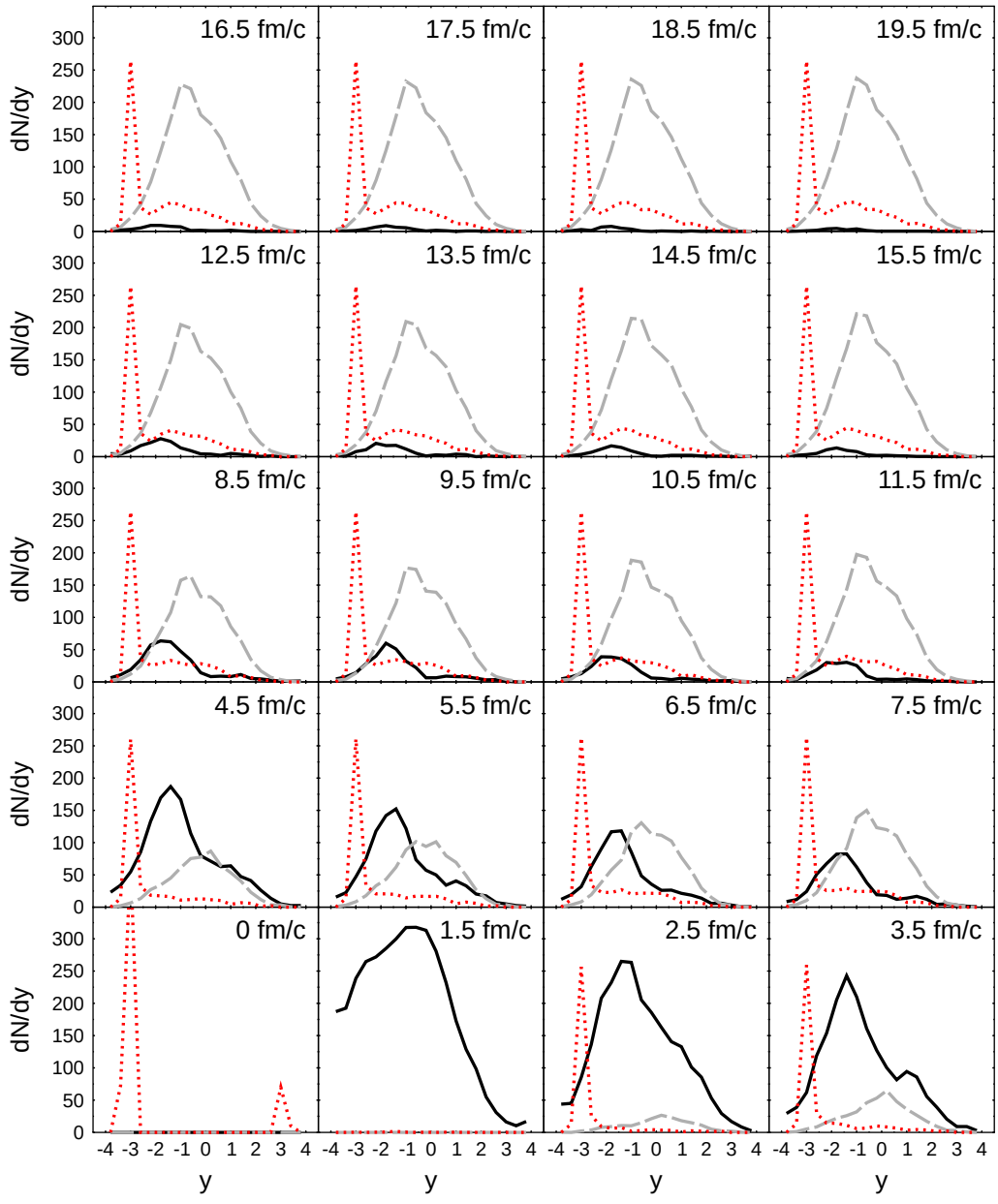

Figure 2: Time evolution of the rapidity distributions of baryons (dotted lines), quarks and antiquarks (solid line) and mesons (dashed line) in a central S+Au collision at SPS (200 GeV/N).

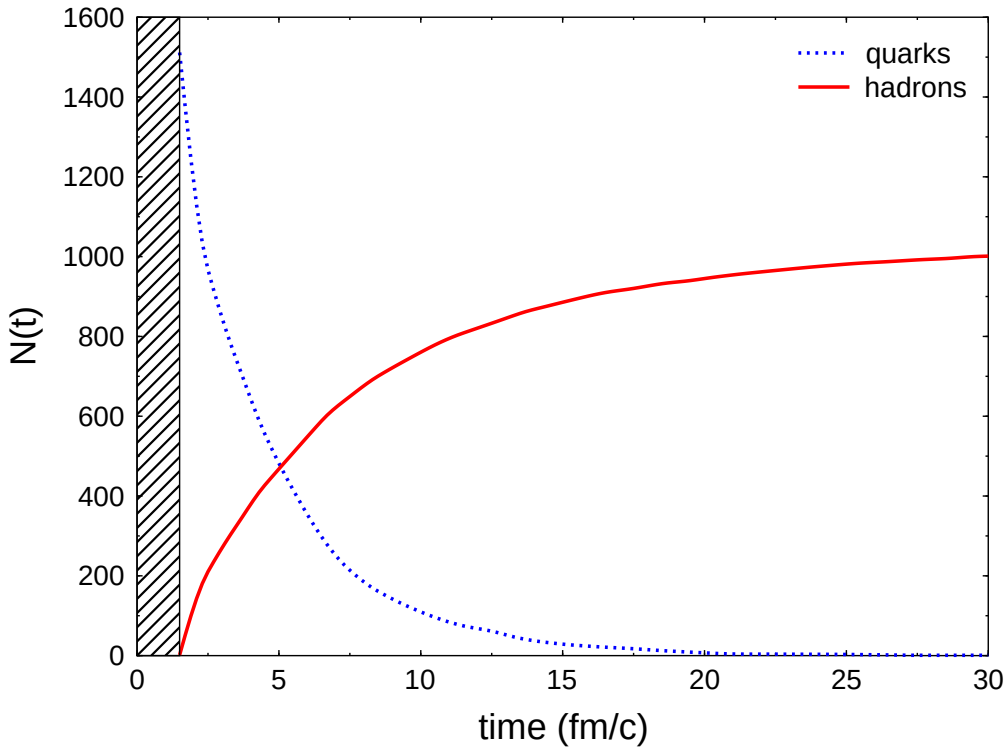

Figure 3: Time evolution of the total number of (anti)quarks and hadrons in the system.

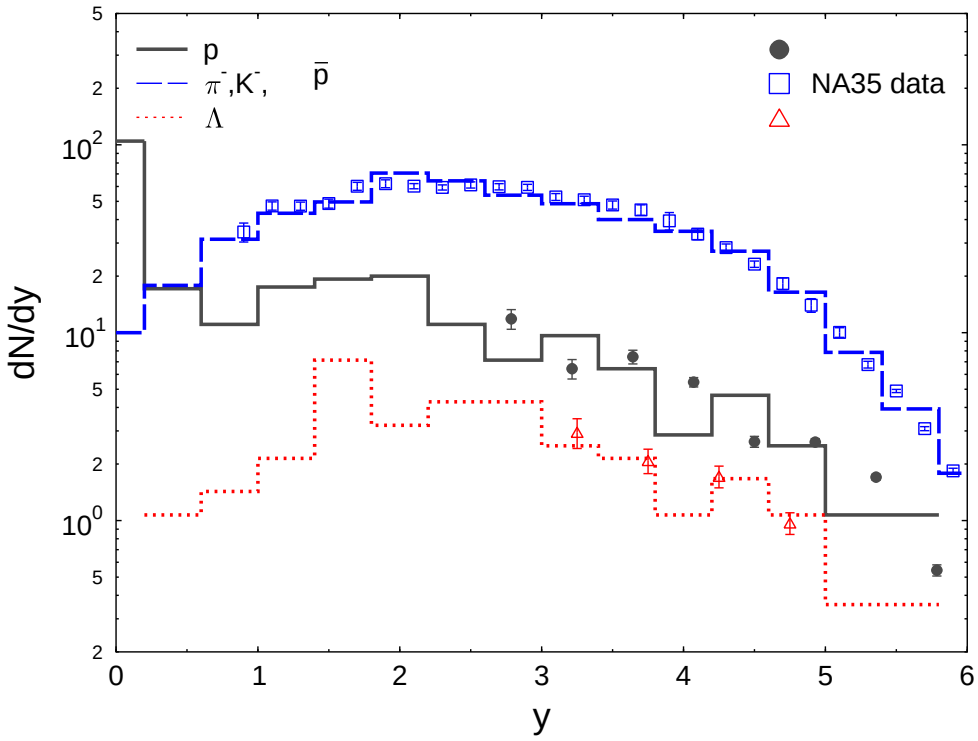

Figure 4: Rapidity distributions of protons, Λ's and h^- in central S+Au collisions at SPS (200 GeV/N) compared to NA35 data [28].

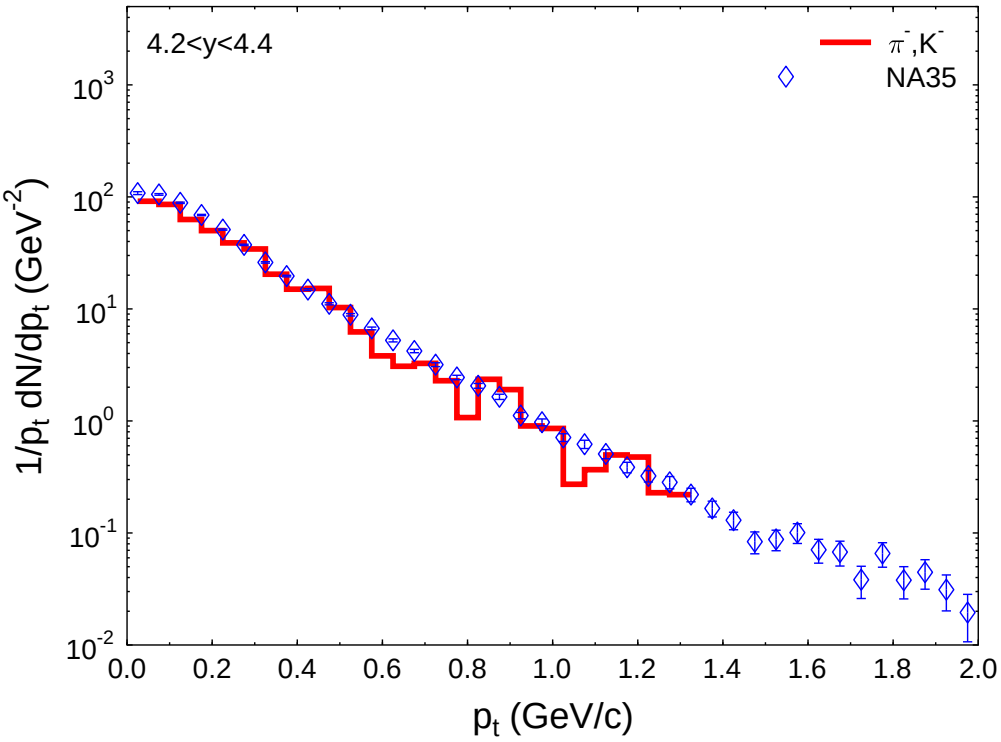

Figure 5: Transverse mass spectrum of negative charged hadrons in central S+Au collisions at SPS (200 GeV/N) compared to NA35 data [28].

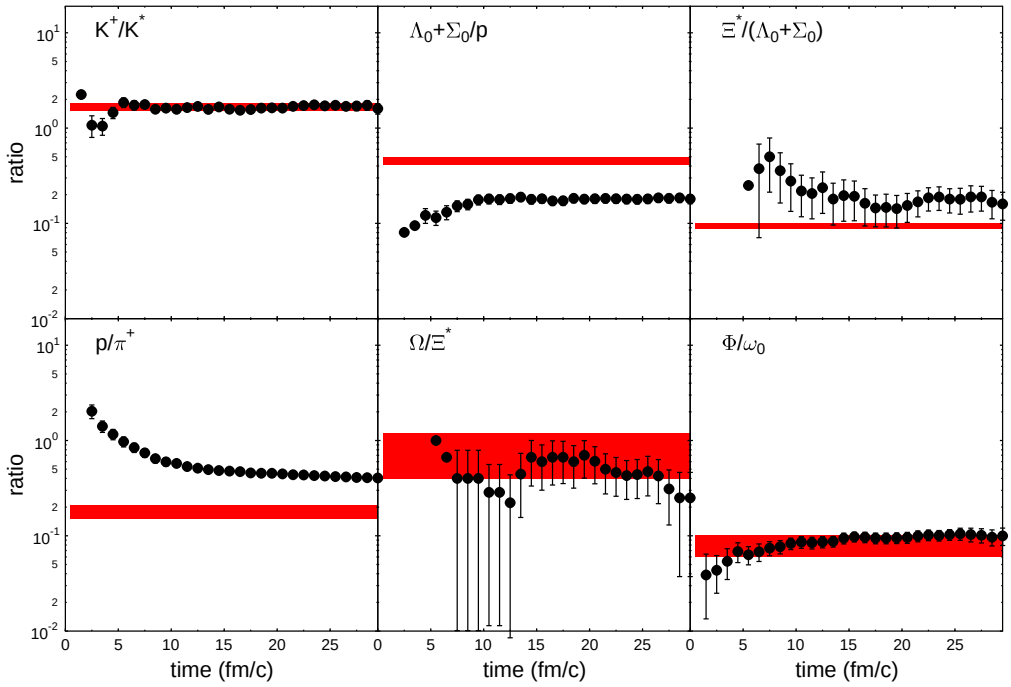

Figure 6: Time evolution of the particle ratios in central S+Au collisions at SPS (200 GeV/N). The shaded areas indicate data taken from [28].

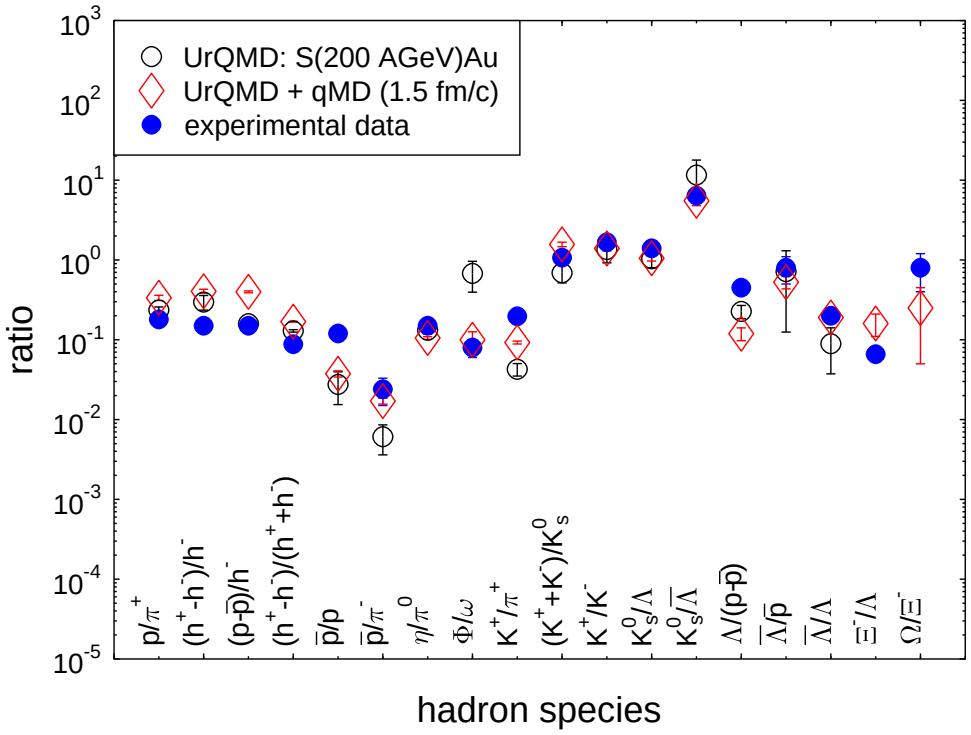

Figure 7: Particle ratios in central S+Au collisions at SPS (200 GeV/N). Experimental data are taken from [28].

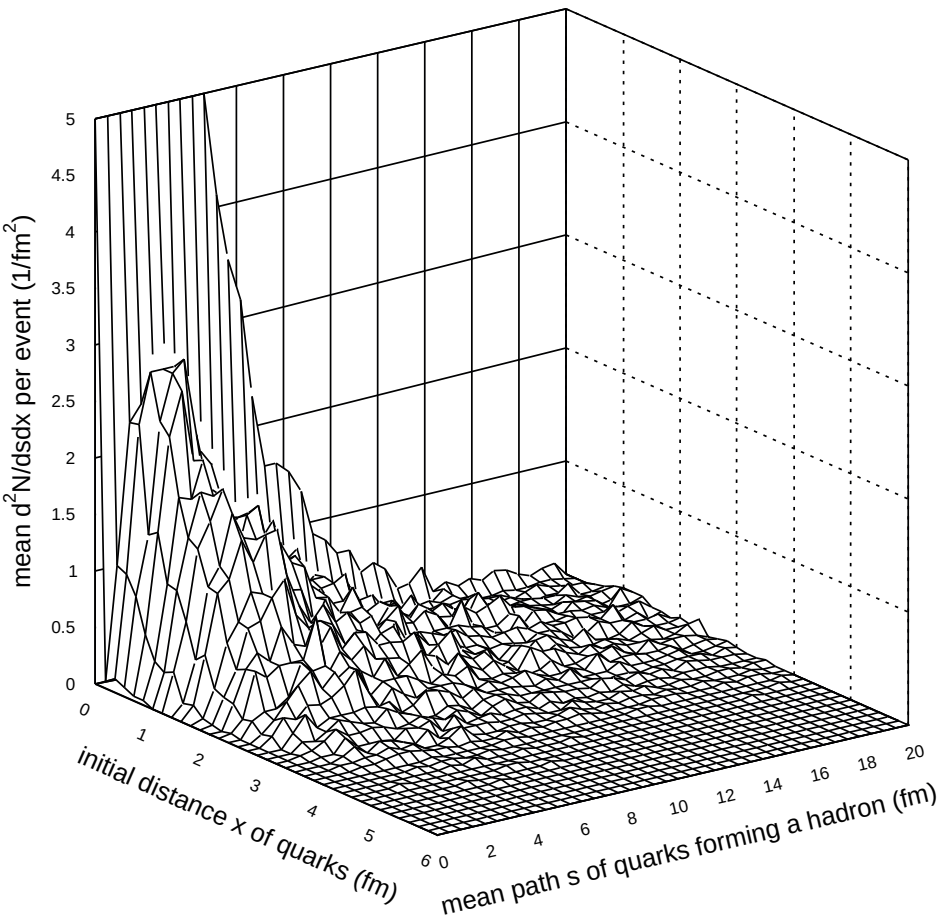

Figure 8: Hadronization in S+Au collisions at SPS (200 GeV/N): Number density distribution of mean diffusion path and initial distance of quarks forming a hadron within qMD.

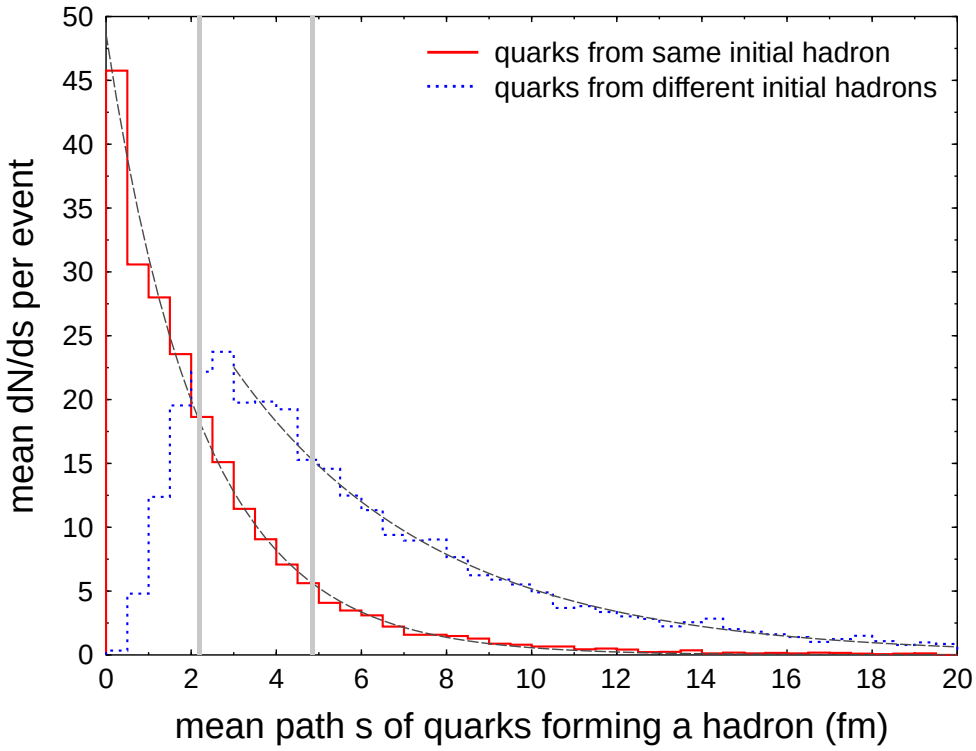

Figure 9: Hadronization in S+Au collisions at SPS (200 GeV/N): Number density distribution of mean diffusion path of quarks forming a hadron from the same initial hadron (solid line) and from different initial hadrons (dashed line) within qMD. Fitting the decay profiles yields diffusion lengths of 2.2 fm and 4.8 fm, respectively